Angewandte Chemie
Eine Zeitschrift der Gesellschaft Deutscher Chemiker

Supporting Information

A Binary Bivalent Supramolecular Assembly Platform Based on Cucurbit[8]uril and Dimeric Adapter Protein 14-3-3

Pim J. de Vink, Jeroen M. Briels, Thomas Schrader, Lech-Gustav Milroy, Luc Brunsveld, and Christian Ottmann**

anie_201701807_sm_miscellaneous_information.pdf

Table of Contents

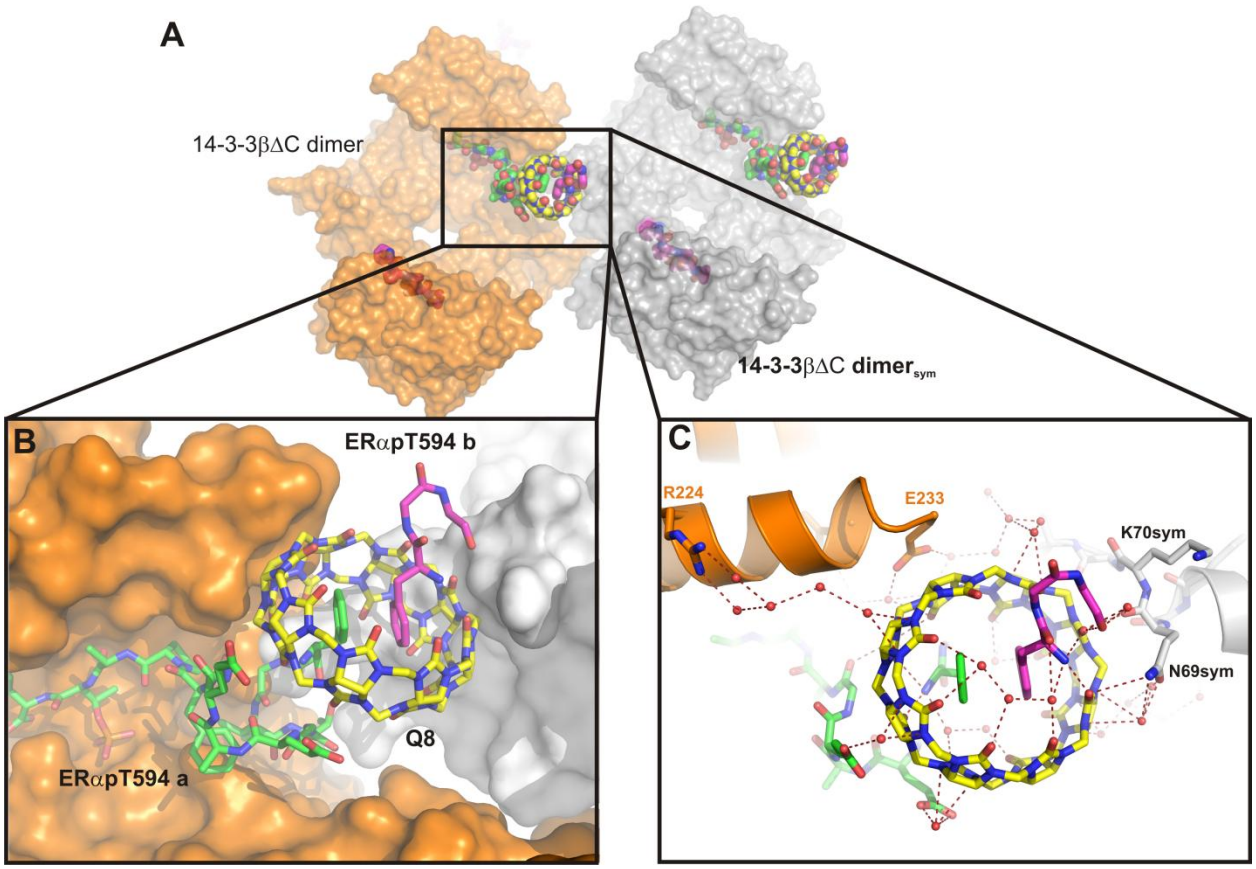

Supporting Figure 1. Stabilization of Q8 binding by a symmetry-related 14-3-3β dimer. (A) Overview, showing the accommodation of phosphorylated sequences in the binding grooves of all 14-3-3 monomers and Q8 bound to both peptides. (B) Q8 (yellow) accommodating the FGG motifs of two FGG-ERα peptides (green and magenta, respectively) and binding to a crystal contact surface between two symmetry-related 14-3-3β dimers (orange and white surface, respectively). (C) Network of water molecules (red spheres) maintaining the polar contacts, mostly hydrogen bonding, (red dotted lines) between Q8, the two FGG-ERα peptides and the two symmetry-related 14-3-3β dimers.

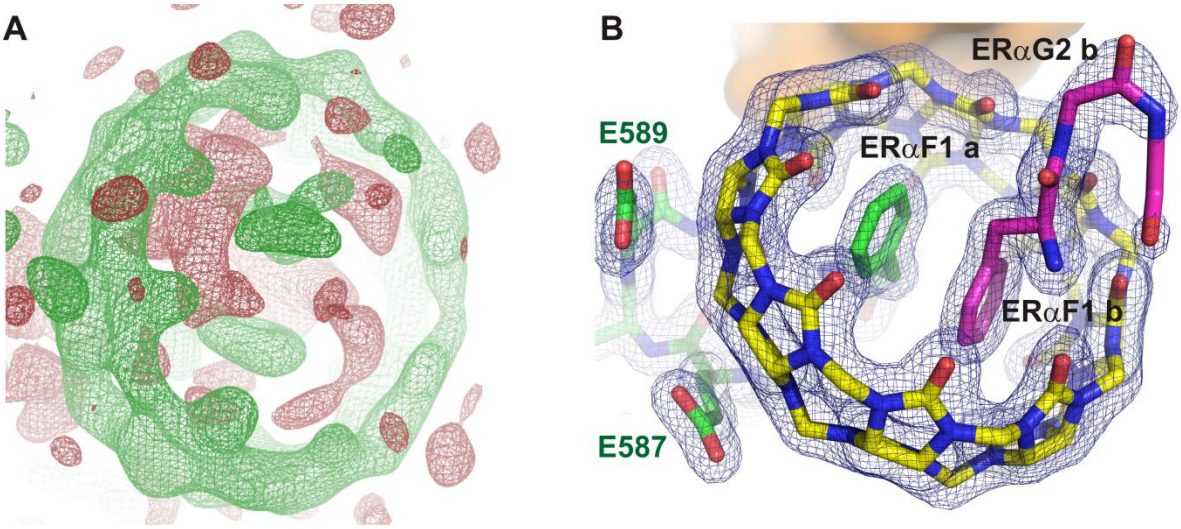

Supporting Figure 2.
Electron densities of Q8. A) Initial electron density map of Q8. B) Final 2Fo-Fc electron density map (contoured at 1σ) of Q8 (yellow sticks) complexed to the FGG-motifs of two FGG-ERα peptides (green and magenta sticks, respectively).

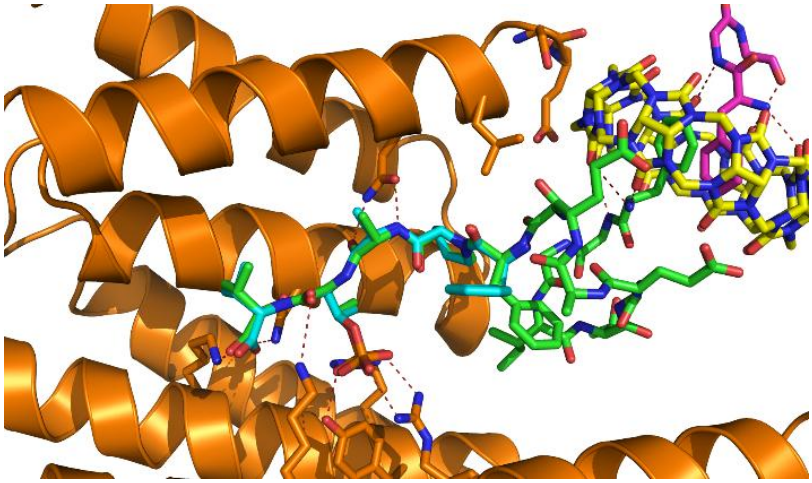

Supporting Figure 3. Overlay of canonical 14-3-3 binding via the phosphorylated motif of the Q8 bound FGG-ERα peptide (green) and the previously crystallized natural ERα peptide sequence (blue). 14-3-3 binding is not hindered by the Q8 complexation. The complexation by Q8 leads to a further structuring / rigidification of the peptide sequence, allowing full molecular resolution of one FGG-ERα peptide (green).

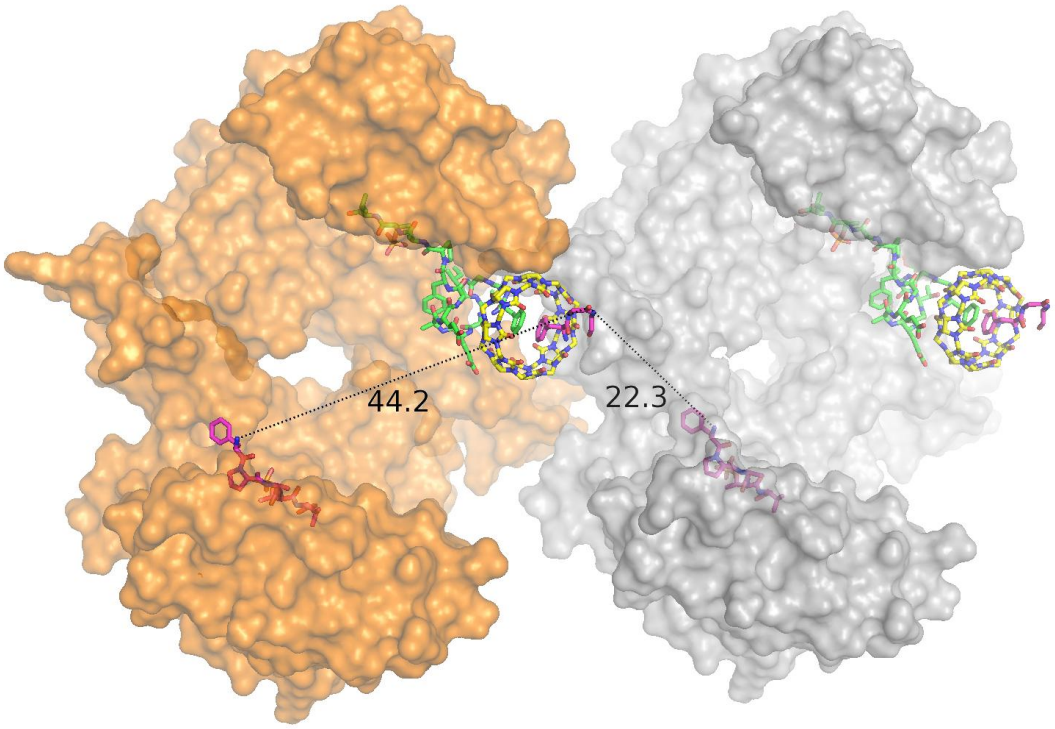

Supporting Figure 4. Distances (in Å) between the *N*-termini of the second, Q8-accommodated FGG-ERα peptide and the *C*-terminal, ERα peptides bound either in the same 14-3-3 (orange surface) dimer, or the symmetry-related 14-3-3 protein (white surface).

Analysis of the supramolecular protein complex

The distance between the third amino acid of the second peptide (magenta, Supporting Figure 4) protruding from Q8 and the N-terminus of the FGG-ERα peptide (F591) of the second protomer of the same 14-3-3 dimer is 44 Å. This distance is too long to be spanned by the 9 remaining, non-visible, amino acids between these positions. The distance between the corresponding positions involving the N-terminus of the peptide binding in the symmetry-related 14-3-3 protein is only 22 Å, a distance that could easily be covered by these 9 amino acids. The interpretation is thus that the second peptide coordinated by Q8 is binding with its C-terminus in the symmetry-related 14-3-3 protein. This constellation is most probably due to the geometry of the crystal lattice, with Q8 as an essential part of the crystal contacts, and the high local concentration of the molecular components in the crystal, and does not necessarily reflect the exact binding conditions in solution.

The supramolecular protein complex was analyzed using the PyMOL Molecular Graphics System, Version 0.99a Schrödinger, LLC and, for distance measurements and structure overlays and VMD, visual molecular dynamics, Version 1.9.2, University of Illinois[1] for determining interfaces of protein–host and protein-protein contracts within the crystal. The interface areas reported in Supporting Table 1 were calculated by comparing the solvent-accessible surface area (SASA) using a probe of 1.4 Å, equal to the radius of a water molecule, of a complex AB with the SASA's individual components A and B using the equation $(A_{SASA} + B_{SASA} – \text{Complex } AB_{SASA})/2$.

Supporting Table 1: Interface size of contracts within the crystal structure

	14-3-3βΔC dimer / Å²	**14-3-3βΔC dimer$_{Sym}$ / Å²**	**Cucurbit[8]uril / Å²**
14-3-3βΔC dimer	-	391.9	125.5
14-3-3βΔC dimer$_{Sym}$	391.9	-	307.9
Cucurbit[8]uril	125.5	307.9	-

Experimental details

Materials

Protein expression and purification was performed as described previously[2]. Cucurbit[8]uril (Q8), Cucurbit[7]uril (Q7), and acridine orange (AO) were obtained via Sigma-Aldrich. The exact concentration of Q8 was determined by titration as described by Kaifer et.al.[3].

Solid-phase peptide synthesis

All peptides were synthesized via Fmoc solid-phase peptide synthesis (SPPS) using an automated Intavis MultiPep RSi peptide synthesizer. TentaGel R RAM resin (Rapp Polymere; 0.18 mmol/g loading) was used for the synthesis of the peptides. Fmoc-protected amino acid building blocks (Novabiochem®) were dissolved in *N*-methylpyrrolidone (NMP) and coupled sequentially by double coupling to the resin using *N*,*N*-diisopropylethylamine(DIPEA)/(2-(1*H*-benzotriazol-1-yl)-1,1,3,3-tetramethyluronium hexafluorophosphate) (HBTU) (4:1 v/v). Fmoc-deprotection was achieved using 20% piperidine in NMP. The control peptides were *N*-terminally acetylated (1:1:3 Ac_2O/pyridine/ NMP) before resin cleavage. The peptide used for FP-assays were labeled with FITC (Sigma-Aldrich) attached to a short polyethylene glycol-based linker introduced via Fmoc-O1pen-OH (Iris Biotech) following reported procedures[4]. Resin cleavage of the protected peptide was performed using 2.5%/2.5%/95% H_2O/triisopropylsilane (TIS)/ trifluoroacetic acid (TFA) and precipitated in cold diethylether. The resultant crude was then re-dissolved in acetonitrile/water/0.1%TFA and lyophilized.

All peptides were further purified by preparative reversed-phase high performance liquid chromatography (HPLC) with MS-detection using a Shimadzu HPLC on a Atlantis® T3 prep OBD C18 column (19x150 mm) with an eluent flow rate of 15 mL/min (MeCN/H_2O/0.1%TFA).

The purity was established by analytical reverse-phase HPLC-MS using a Shimadzu HPLC on a Atlantis® T3 C18 analytical column (2.1x150 mm) LCQ Fleet from Thermo Scientific, Surveyor AS and PDA with an eluent flow rate of 0.2 mL/min (MeCN/H_2O/0.1%TFA) 0-1 min, isocratic, 5% acetonitrile (MeCN); 1-10 min, linear gradient, 5-70%; 10-11 min, isocratic, 70%; 11- 12 min, linear gradient, 70-5%; 12-15 min, isocratic, 5% MeCN.

Fluorescence Polarization Assays

All fluorescence anisotropy affinity measurements were performed using a filter-based microplate reader (Tecan Infinite F500) using a fluorescein filterset (λ_{ex}:485 nm/20 nm, λ_{em}:535 nm/25 nm) and an integration time of 50 µs in black, round-bottom 384microwell plates with wells of a volume of 10µL (Corning, #25916024) in triplicate at 20°C. The data was fitted using GraphPad Prism 5.05 for Windows (GraphPad Software Inc., CA, USA four-parameter logistic model (4PL) according to precedent from our group[5,6].

The fluorescein (FITC)-labelled bivalent ExoS-peptide (fBiExoS) used in the competition fluorescence anisotropy studies – (5,6-FITC-O1Pen-QGLLDALDLAS(GGSGGGGSGG)QGLLDALDLAS-NH_2) – was dissolved in HEPES buffer (10mM HEPES, pH 7.4, 150mM NaCl), to a concentration of 50 µM with a set pH of 7.4, aliquoted, flash-frozen in liquid nitrogen and stored at 243 K. The FITC-labelled monovalent ExoS-peptide (FITC-MonoExoS; 5,6-FITC-O1Pen-QGLLDALDLAS-NH_2) was used as reference (Supporting Figure 5).

Direct FP measurements for determining ExoS-peptide affinity to 14-3-3 were performed using 10nM fluorescein-labeled bivalent ExoS-peptide in FP-buffer containing 10mM HEPES (pH 7.4), 150mM NaCl, 0.01% (v/v) TWEEN20 and 0.1% (w/v) BSA by a dilution series varying the concentration of 14-3-3β protein (Supporting Figures 5 and 6).

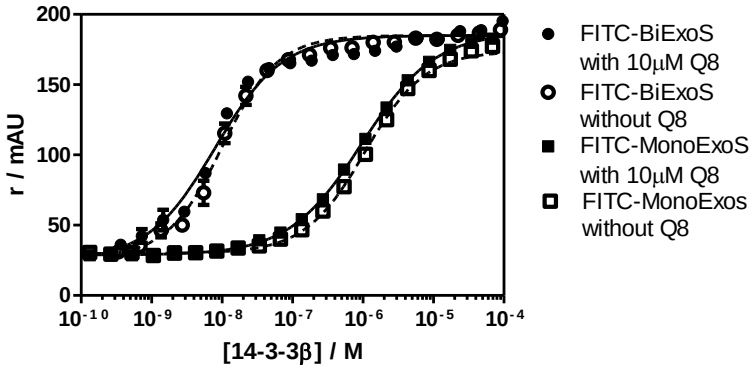

Supporting Figure 5. Direct FP titration of 14-3-3β protein to FITC-BiExoS (10 nM) and FITC-MonoExoS (10 nM) without and with 10uM Q8 in FP-Buffer (10 mM HEPES, pH 7.4, 150 mM NaCl, 0.01% TWEEN20, 1 mg/mL BSA) at 20°C. Q8 does not influence ExoS peptide binding to 14-3-3.

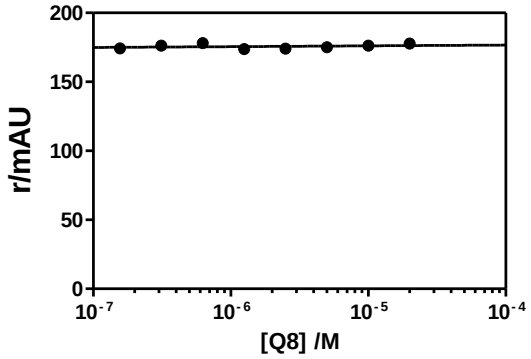

Supporting Figure 6. Fluorescence polarization titration of Q8 to 10 nM FITC-BiExoS and 40nM 14-3-3β in FP-Buffer (10 mM HEPES, pH 7.4, 150 mM NaCl, 0.01% TWEEN20, 1 mg/mL BSA) at 20°C. Q8 does not influence ExoS peptide binding to 14-3-3.

Fluorescence Depolarization Assays

Competition FP measurements (Figure 2 main manuscript) were performed using 10 nM fluorescein-labeled bivalent ExoS-peptide and 40nM 14-3-3β in FP-buffer containing 10 mM HEPES (pH 7.4), 150 mM NaCl, 0.01% (v/v) TWEEN20 and 0.1% (w/v) BSA. Dilution series were made varying the concentration of FGG-ERα-peptide with several constant concentrations of Q8 and Q7 (Figures 2B, C, E). In addition, dilution series were made varying the concentration of Q8 with several constant concentrations FGG-ERα-peptide (Figure 2D).

Fluorimetric Assays

All fluorimetric assays were performed using a filter-based microplate reader (Tecan Infinite F500) using a filterset (λ_{ex}:485 nm/20 nm, λ_{em}:535 nm/25 nm) and an integration time of 50 µs in black, round-bottom 384microwell plates with wells of a volume of 10µL (Corning, #25916024) in triplicate at 20°C. The data was fitted using GraphPad Prism 5.05 for Windows (GraphPad Software Inc., CA, USA four-parameter logistic model (4PL).

Direct fluorimetric titrations were performed for determining Acridine Orange (AO) affinity for Q8 and potential background binding to 14-3-3 using 1 µM acridine orange hydrochloride hydrate (AO) (Sigma-Aldrich) in FP-buffer containing 10mM HEPES (pH 7.4), 150mM NaCl, 0.01% (v/v) TWEEN20 and 0.1% (w/v) BSA by a dilution series varying the concentration of Q8 and without and with 10 µM 14-3-3β.

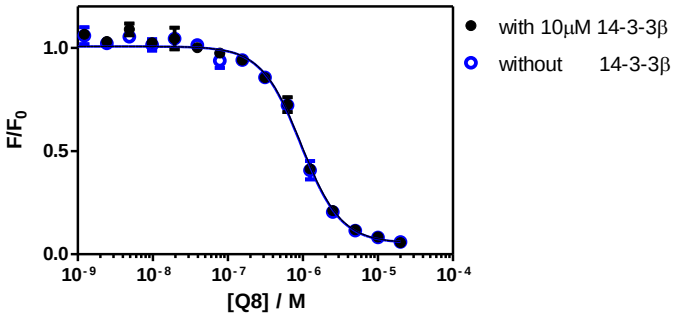

Supporting Figure 7. Direct titration of cucurbit[8]uril (Q8) to acridine orange AO (1 µM) with 10 µM 14-3-3 β and without 14-3-3β in FP-Buffer (10 mM HEPES, pH 7.4, 150 mM NaCl, 0.01% TWEEN20, 1 mg/mL BSA). Q8 binding to AO is independent of the presence of 14-3-3.

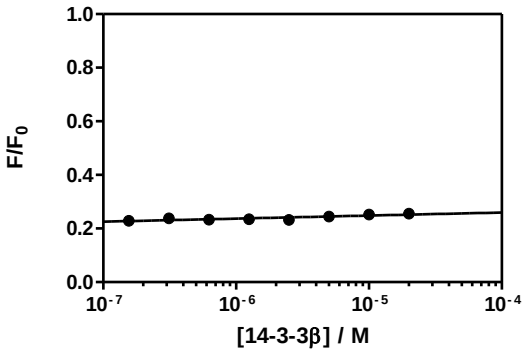

Supporting Figure 8. Fluorimetric titration series of 14-3-3β to acridine orange (1µM) and Q8 (1µM) in FP-Buffer (10 mM HEPES, pH 7.4, 150 mM NaCl, 0.01% TWEEN20, 1 mg/mL BSA) at 20°C. Q8 binding to AO is independent of the presence of 14-3-3.

Fluorimetric Displacement Assay

For the fluorimetric displacement assay (Figure 3 main manuscript), solutions of acridine orange hydrochloride hydrate (1 µM) (Sigma-Aldrich) and cucurbituril (1 µM) in FP Buffer (10 mM HEPES, pH 7.4, 150 mM NaCl, 0.01% TWEEN 20, 1 mg/mL BSA) with different set concentrations of 14-3-3β were titrated with varying concentrations of FGG-ERα-peptide.

Asymmetric Flow Field-Flow Fractionation (AF4)

The asymmetric flow field-flow fractionation - UV - QELS (AF4-UV- QELS) experiments were performed on a Wyatt Eclipse AF4 instrument connected to a Shimadzu LC-2030C 3D, with an internal PDA. The AF4 was further connected to the following detectors: a WYATT:DAWN HELEOS II light scattering detector (MALLS) using a laser operating at 658nm and a Wyatt Optilab Rex refractive index detector. Detectors were normalized using Bovine Serum Albumin and for protein molecular weight calculations, dn/dc of 0.1850 was used. All AF4 fractionations were performed on an AF4 short channel with regenerated cellulose (RC) 10 KDa membrane (Millipore) and spacer of 350 µm. The AF4 channel was pre-washed with running solution of 10 mM phosphate buffer (pH 7.2). This solution was also used as eluent with 0.8mL/min detection flow, 2mL/min focus flow and 1.8mL/min 0-2min equilibration, 2-3 min focus, 3-6 min focus and inject, 6-7minute focus, 7-22 elution, 22-25 wash. Samples of 10 µL BSA (75 µM), and of 50 µL 14-3-3β (40 µM), 14-3-3β:FGG-ERα peptide (40 µM:100 µM), and 14-3-3β:FGG-ERα peptide:Q8 (40 µM:100 µM:40 µM) were run. The processing and analysis of the LS data and radius of hydration (R_H) calculations were performed on Astra 7.0.1. All 14-3-3 complexes show a single peak in the DRI fractograms with a retention time around 11.5 minutes (Supporting Figure 9), representing a single type of particle. The AF4-QELS trace (Supporting Figure 10) around the peak maxima (~11.5 min.) of 14-3-3 reveal the formation of compact particles of around 3 nm with an apparent small increase in R_H upon complexation with the FGG-ERα peptide, or FGG-ERα peptide and Q8 (Supporting Table 2).

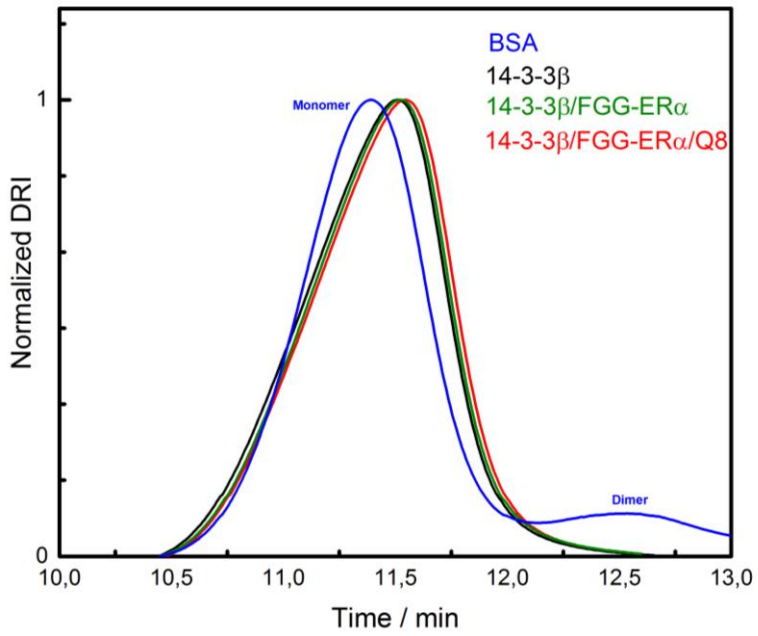

Supporting Figure 9. DRI fractograms of BSA (75 µM), 14-3-3β (40µM), 14-3-3β:FGG-ERα peptide (40 µM:100 µM), and 14-3-3β:FGG-ERα peptide:Q8 (40 µM:100 µM:40 µM)

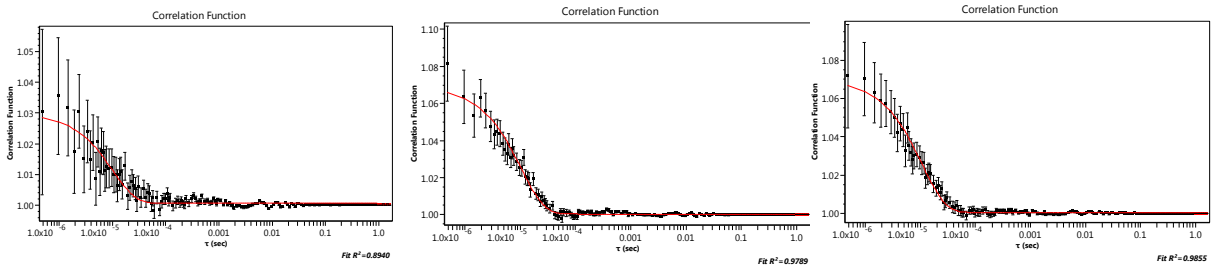

Supporting Figure 10. AF4-QELS traces of 14-3-3β (left), 14-3-3β:FGG-ERα peptide (middle), 14-3-3β:FGG-ERα peptide:Q8 (right).

Supporting Table 2. Calculated Radii of hydration, based on AF4-QELS traces.

Protein	R_H (nm)
14-3-3β	2.99 ± 1.00
14-3-3β + FGG-ERα	3.00 ± 0.43
14-3-3β + FGG-ERα + Q8	3.14 ± 0.44

Crystallography X-ray experiments

A solution of 600µM 14-3-3βΔC, 600µM Q8 and 1500µM FGG-ERα peptide was incubated overnight in size exclusion buffer (10mM TRIS, 150mM NaCl, 5mM 2-mercapto-ethanol). Crystal were obtained at 4°C in 1.36 M sodium citrate at pH 6.0 with 15% (v/v) PEG1500 in the course of four weeks. The crystals were transferred into crystallization buffer supplemented with 30% glycerol and flash-cooled in liquid nitrogen. The diffraction pattern was collected at a synchrotron source to a resolution of 1.67 Å at the SLS beamline. Molecular replacement was done using the CCP4i software package[7] from the 14-3-3β crystal structure, refinement and model building were done with the Phenix[8] and COOT[9] software packages.

Data processing and refinement statistics

RMS bond lengths and angle is RMSD from ideal geometry values. Data were collected from a single crystal. a) Values in parentheses are for highest resolution shell used in the refinement.

Supporting Table 3. XRD dataset statistics	
PDB ID	5N10
Data collection	
Beam line	PXII-X10SA at SLS
Wavelength (Å)	0.978
Resolution (Å)	66.14-1.07 (1.63-1.60)
Space group	C121
Cell dimensions	
a, b, c, (Å)	133.81, 57.57, 93.45
α, β, γ, (°)	90.00, 98.64, 90.00
Total reflections[a]	620401 (30008)
Unique reflections[a]	92397 (4508)
Redundancy[a]	6.7 (6.7)
Completeness (%)[a]	99.6 (99.0)
Average I/σ(I)[a]	13.5 (1.4)
Wilson B-factor	19.8
$CC_{1/2}$[a]	0.999 (0.554)
R_{sym}[a]	0.074 (1.444)
R_{meas}[a]	0.080 (1.565)
Refinement	
Reflections used in refinement	92384
Reflections used for R-free	1922
Non-hydrogen atoms (protein / solvent)	4355 / 563
R_{work} (%)	16.96
R_{free} (%)	19.35
RMS (bonds) / RMS (angles)	0.011 / 1.182
Average protein B-factor	38
Ramachandran: favored / outliers (%)	99.24 / 0.00
Clash score	3.52

LCMS-Traces

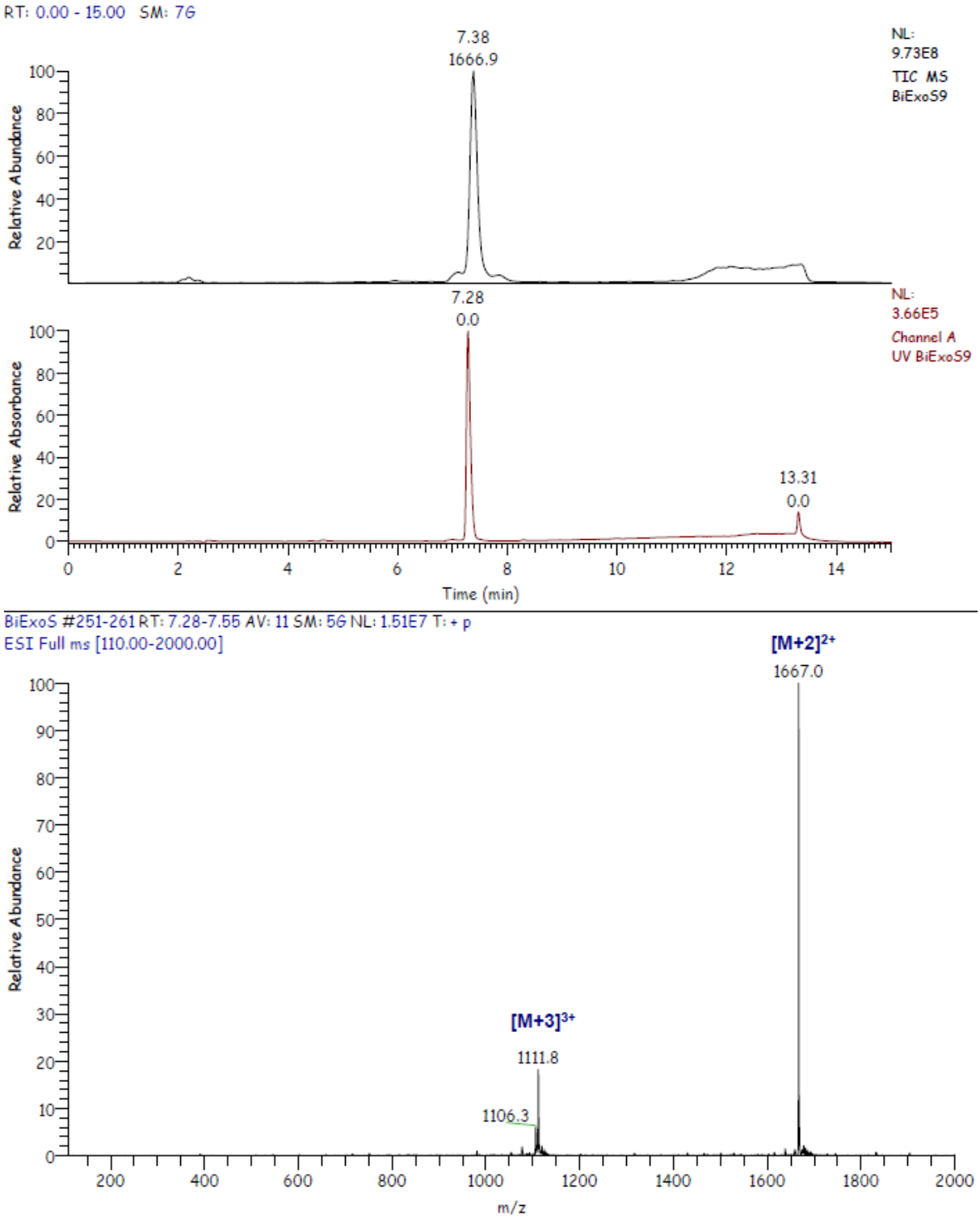

Supporting Figure 11. Analytical data for fBiExoS: FITC-O1Pen-QGLLDALDLAS(GGSGGGGSGG)QGLLDALDLAS-NH_2, Rt=7.4; ESI-MS: $[M+2H]^{2+}$ calculated 1667.2, observed 1667.0; $[M+3H]^{3+}$, calculated 1111.8, observed 1111.8.

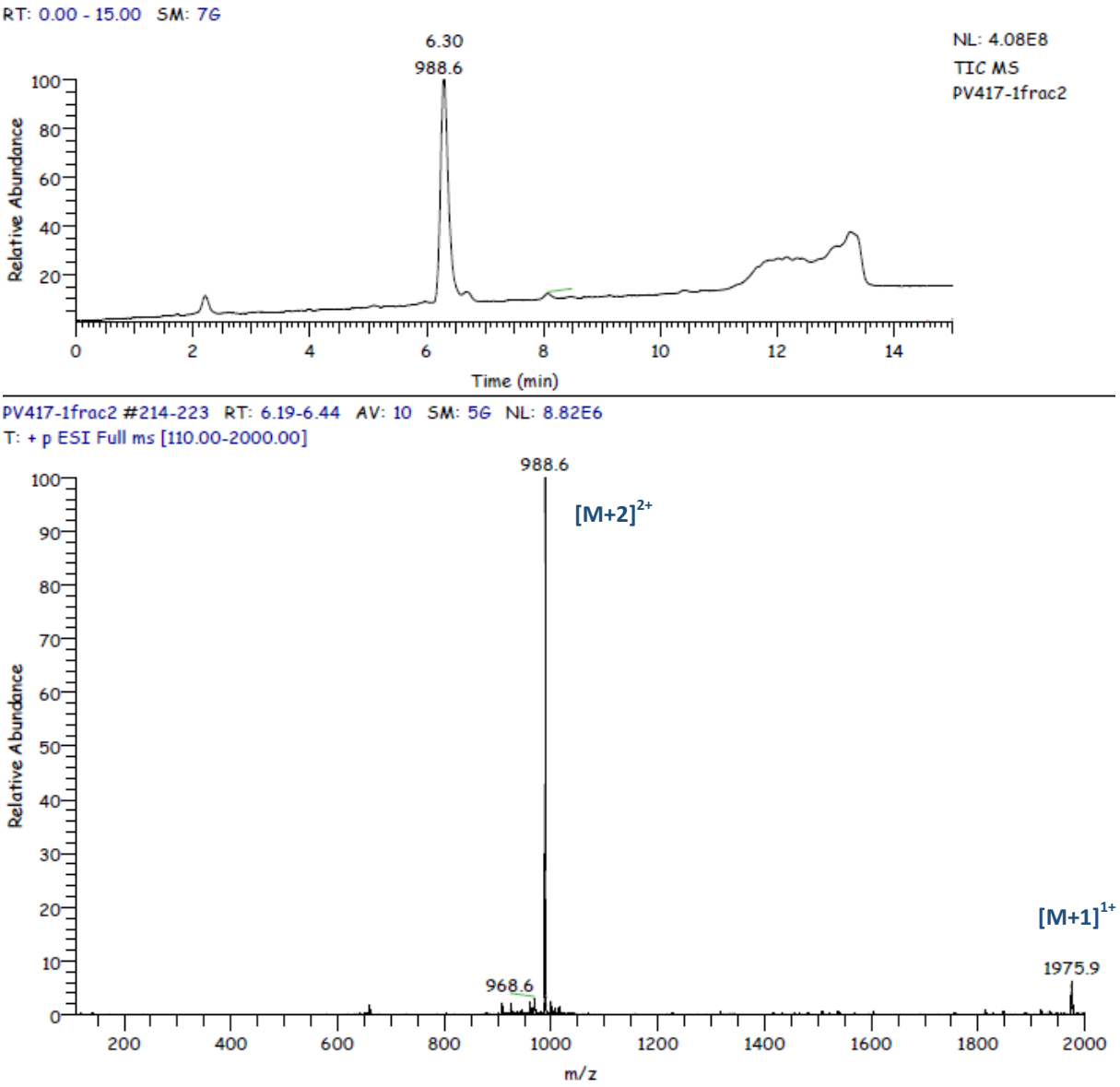

Supporting Figure 12. Analytical data for fMonoExoS: FITC-O1Pen-QGLLDALDLAS-NH_2, Rt=6.3; ESI-MS: $[M+1H]^{1+}$, calculated 1760.1, observed 1775.9; $[M+2H]^{2+}$ calculated 988.5, observed 988.6;

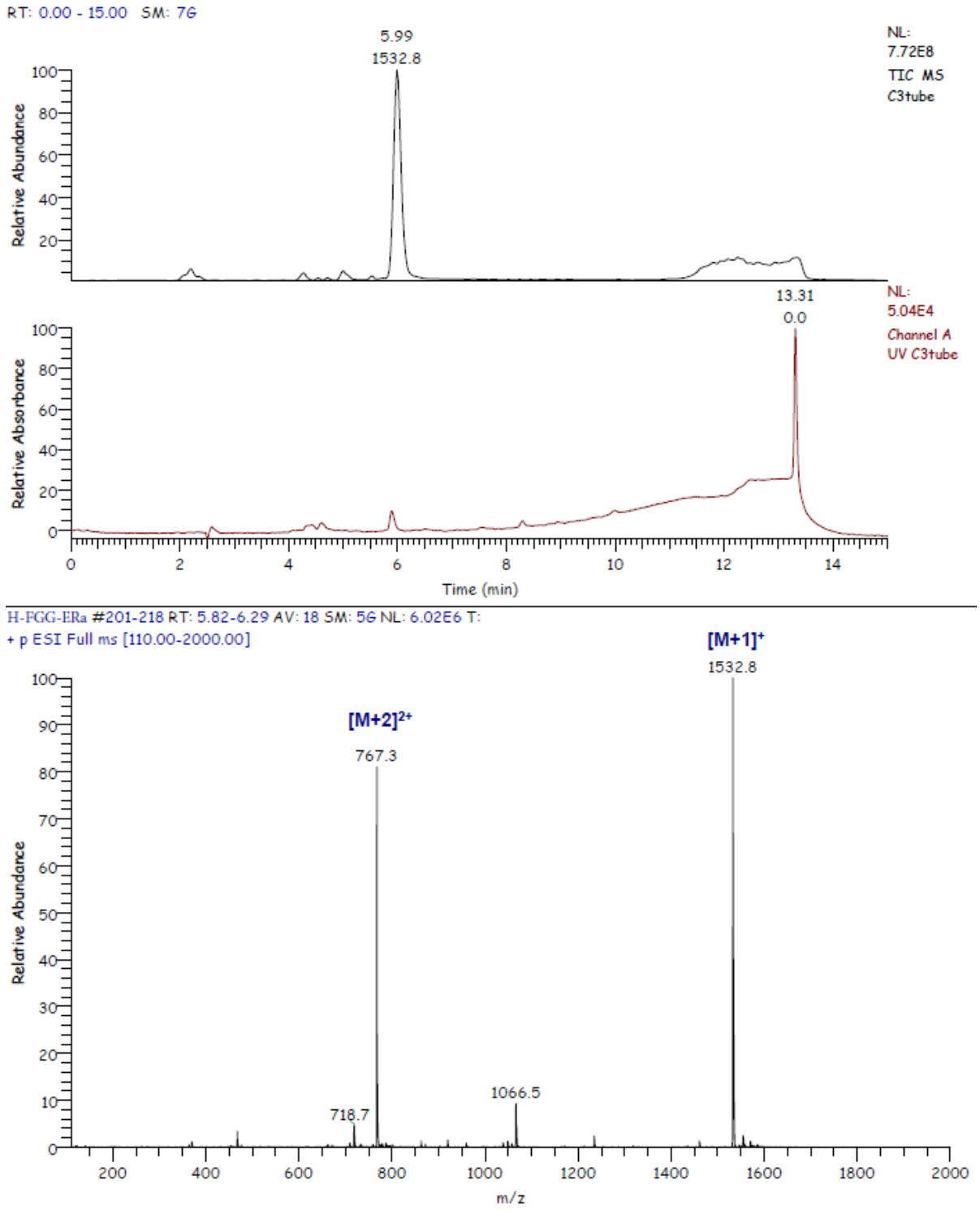

Supporting Figure 13 Analytical data for H-FGG-ERα: *H*-FGG-ITGEAEGFPApTV-*OH*, R=6.0; ESI-MS: $[M+H]^+$ calculated 1532.6, observed 1532.8; $[M+2H]^{2+,}$ calculated 766.8, observed 767.3;

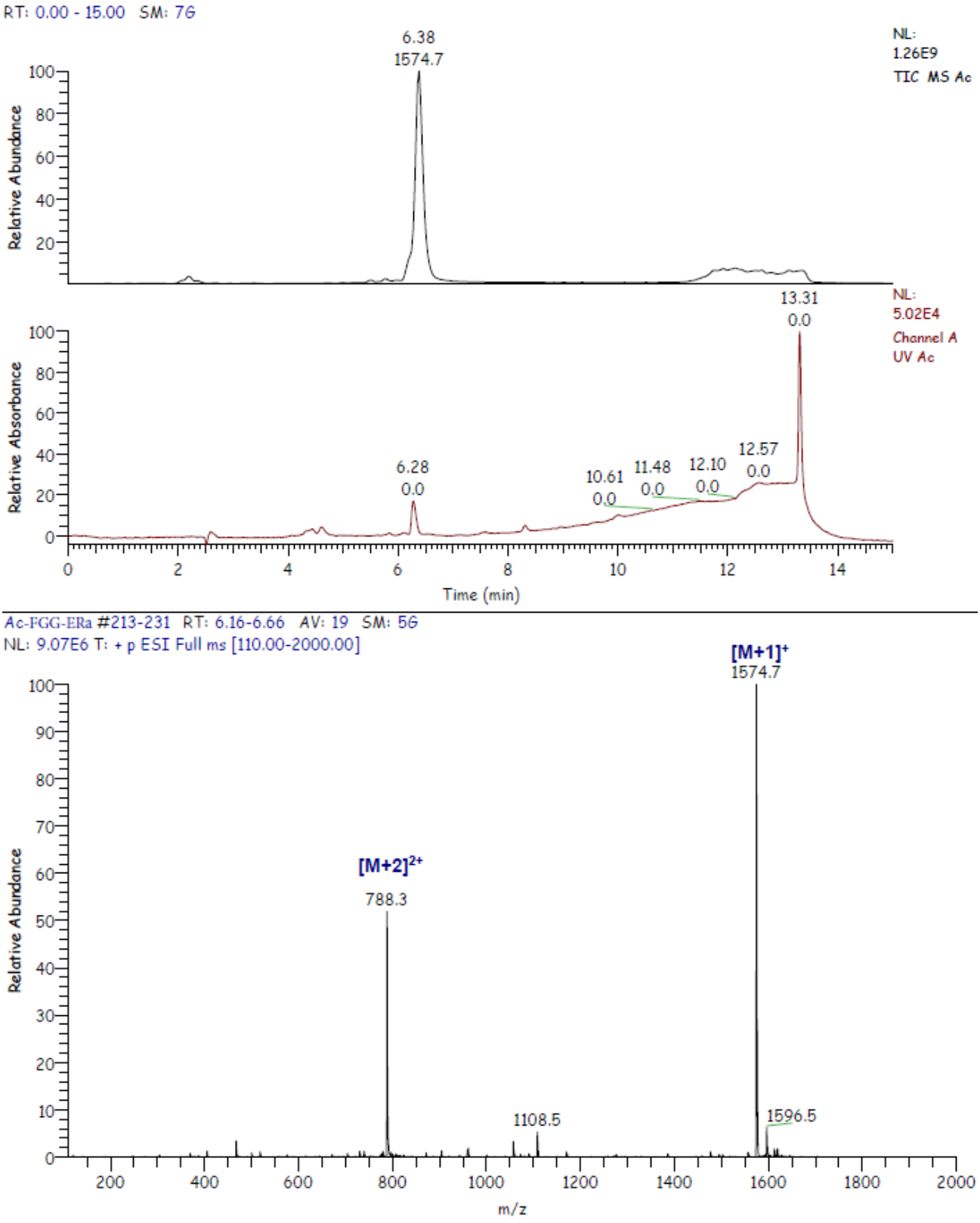

Supporting Figure 14. Analytical data for Ac-FGG-ERα: *Ac*-FGG-ITGEAEGFPApTV-*OH*, R=6.4; ESI-MS: $[M+H]^+$ calculated 1574.6, observed 1574.7; $[M+2H]^{2+}$, calculated 787.8, observed 788.3;

Supporting References

[1] W. Humphrey, A. Dalke, K. Schulten, *J. Mol. Graph.* **1996**, *14*, 33–38, 27–28.
[2] L. M. Stevers, C. V. Lam, S. F. R. Leysen, F. A. Meijer, D. S. van Scheppingen, R. M. J. M. de Vries, G. W. Carlile, L. G. Milroy, D. Y. Thomas, L. Brunsveld, et al., *Proc. Natl. Acad. Sci.* **2016**, *113*, E1152–E1161.
[3] S. Yi, A. E. Kaifer, *J. Org. Chem.* **2011**, *76*, 10275–10278.
[4] Y.-W. Kim, T. N. Grossmann, G. L. Verdine, *Nat Protoc.* **2011**, *6*, 761–771.
[5] D. Bier, R. Rose, K. Bravo-Rodriguez, M. Bartel, J. M. Ramirez-Anguita, S. Dutt, C. Wilch, F.-G. Klärner, E. Sanchez-Garcia, T. Schrader, et al., *Nat Chem* **2013**, *5*, 234–239.
[6] L.-G. Milroy, M. Bartel, M. A. Henen, S. Leysen, J. M. C. Adriaans, L. Brunsveld, I. Landrieu, C. Ottmann, *Angew. Chem. Int. Ed.* **2015**, *54*, 15720–15724.
[7] M. D. Winn, C. C. Ballard, K. D. Cowtan, E. J. Dodson, P. Emsley, P. R. Evans, R. M. Keegan, E. B. Krissinel, A. G. W. Leslie, A. McCoy, et al., *Acta Crystallogr. Sect. D* **2011**, *67*, 235–242.
[8] P. D. Adams, R. W. Grosse-Kunstleve, L.-W. Hung, T. R. Ioerger, A. J. McCoy, N. W. Moriarty, R. J. Read, J. C. Sacchettini, N. K. Sauter, T. C. Terwilliger, *Acta Crystallogr. Sect. D* **2002**, *58*, 1948–1954.
[9] P. Emsley, B. Lohkamp, W. G. Scott, K. Cowtan, *Acta Crystallogr. Sect. D* **2010**, *66*, 486–501.